Inorg. Chem. **2009**, *48*, 3783−3791

Trivalent Iron and Ruthenium Complexes with a Redox Noninnocent (2-Mercaptophenylimino)-methyl-4,6-di-*tert*-butylphenolate(2-) Ligand

Nabarun Roy, Stephen Sproules, Thomas Weyhermüller, and Karl Wieghardt*

Max-Planck-Institut für Bioanorganische Chemie, Stiftstrasse 34-36, D-45470 Mülheim an der Ruhr, Germany

Received December 12, 2008

The 3,5-di-*tert*-butyl substituted *N*-(salicylidene)-*o*-mercaptoaniline (H_2L) ligand reacted with equimolar amounts of $FeBr_2$ and 2 equiv of triethylamine in air affords $[Fe^{III}(L-L)Br]^0$ (**1**), where $(L-L)^{2-}$ is a pentacoordinate ligand formed from the oxidative dimerization of L^{2-} via disulfide bridge formation. Reaction of H_2L with $RuCl_3 \cdot H_2O$ and NEt_3 gives a dark green-brown dinuclear complex, $[Ru^{III}_2(L)_2Cl_2(NCCH_3)_2]^0$ (**2**). Both complexes have been characterized by X-ray crystallography. A Ru−Ru single bond is evident in **2**. Complex **1** has also been characterized by electron paramagnetic resonance and Mössbauer spectroscopies and magnetic susceptibility measurements that identify a high-spin Fe(III) ($S = {}^5/_2$) center. Diamagnetic **2** is successively twice reversibly one-electron oxidized to produce $[Ru^{III}_2(L^{\bullet})(L)Cl_2(NCCH_3)_2]^+$, $[\mathbf{2}]^+$ ($S = {}^1/_2$), and $[Ru^{III}_2(L^{\bullet})_2Cl_2(NCCH_3)_2]^{2+}$, $[\mathbf{2}]^{2+}$ ($S = 0$). Spectroelectrochemical and electron paramagnetic resonance measurements identify these as ligand-based oxidations affording *o*-coordinated phenoxyl radicals. DFT calculations on the electron transfer series corroborate this result and that the Ru−Ru single bond is retained throughout this series.

Introduction

Various strategies are used by metalloenzymes to store oxidizing equivalents required for multi-electron transfers. A fascinating class of metalloenzymes uses an organic redox center (free radical) on their own polypeptide chain to provide or abstract electrons and complete metal-driven electron transfer processes.[1] Both galactose oxidase and glyoxal oxidase are examples in point, with the incorporation of a tyrosyl radical into their active site that catalyzes the oxidation of a broad range of primary alcohols to aldehydes with a concomitant reduction of molecular oxygen.[2] The impetus to understand the enzymatic mechanism has instigated the synthesis and characterization of transition metal complexes with *coordinated* phenoxyl radical ligands.[3] To this end, several mimicks utilizing large multidentate ligands possessing pendent phenolate arms have been prepared, and their spectroscopic and X-ray crystallographic characterization has established a set of markers for phenoxyl radical coordination: (i) a short C−O bond (<1.3 Å) indicating significant double bond character with an accompanying semiquinoidal distortion of two short and four long C−C bonds in the phenyl ring,[4−6] (ii) an intense phenoxyl $\pi \rightarrow \pi^*$ transition at ∼400 nm in the UV−vis spectrum,[6−12] (iii) an electron paramagnetic resonance (EPR) spectrum exhibit-

* To whom correspondence should be addressed. E-mail: wieghardt@mpi-muelheim.mpg.de.

(1) Fontecave, M.; Pierre, J. L. *Acad. Sci. Paris Chim.* **2001**, *4*, 531.
(2) Whittaker, J. W. In *Metal Ions in Biological Systems*; Sigel, H., Sigel, A., Eds.; Marcel Dekker: New York, 1994; Vol. *30*, p 315.
(3) (a) Jazdzewski, B. A. T. W. B. *Coord. Chem. Rev.* **2000**, *200*−*202*, 633. (b) Chaudhuri, P.; Wieghardt, K. *Prog. Inorg. Chem.* **2001**, *50*, 151.
(4) Sokolowski, A.; Bothe, E.; Bill, E.; Weyhermüller, T.; Wieghardt, K. *Chem. Commun.* **1996**, 1671.
(5) Benisvy, L.; Blake, A. J.; Collison, D.; Davies, E. S.; Garner, C. D.; McInnes, E. J. L.; McMaster, J.; Whittaker, G.; Wilson, C. *Dalton Trans.* **2003**, 1975.
(6) Benisvy, L.; Blake, A. J.; Collison, D.; Davies, E. S.; Garner, C. D.; McInnes, E. J. L.; McMaster, J.; Whittaker, G.; Wilson, C. *Chem. Commun.* **2001**, 1824.
(7) Adam, B.; Bill, E.; Bothe, E.; Goerdt, B.; Haselhorst, G.; Hildenbrand, K.; Sokolowski, S.; Steenken, S.; Weyhermüller, T.; Wieghardt, K. *Chem.—Eur. J.* **1997**, *3*, 308.
(8) (a) Benisvy, L.; Bill, E.; Blake, A. J.; Collison, D.; Davies, E. S.; Garner, C. D.; Guindy, C. I.; McInnes, E. J. L.; McArdle, G.; McMaster, J.; Wilson, C.; Wolowska, J. *Dalton Trans.* **2004**, 3647. (b) Nairn, A. K.; Archibald, S. J.; Bhalla, R.; Gilbert, B. C.; MacLean, E. J.; Teat, S. J.; Walton, P. H. *Dalton Trans.* **2006**, 172. (c) Nairn, A. K.; Bhalla, R.; Foxon, S. P.; Liu, X.; Yellowlees, L. J.; Gilbert, B. C.; Walton, P. H. *J. Chem. Soc., Dalton Trans.* **2002**, 1253.
(9) Halfen, J. A.; Jazdzewski, B. A.; Mahapatra, S.; Berreau, L. M.; Wilkinson, E. C.; Que, L., Jr.; Tolman, W. B. *J. Am. Chem. Soc.* **1997**, *119*, 8217.
(10) (a) Müller, J.; Kikuchi, A.; Bill, E.; Weyhermüller, T.; Hildebrandt, P.; Ould-Moussa, L.; Wieghardt, K. *Inorg. Chim. Acta* **2000**, *297*, 265. (b) Wang, Y.; DuBois, J. L.; Hedman, B.; Hodgson, K. O.; Stack, T. D. P. *Science* **1997**, *279*, 537.

10.1021/ic8023716 CCC: $40.75
Published on Web 03/20/2009

ing $g \sim 2.004$ with the g anisotropy and nuclear hyperfine dependent on the neighboring nuclei,[7,9,13−15] and (iv) resonance Raman peaks assigned as the ν_{7a} (C−O) and ν_{8a} ($C_{ortho}-C_{meta}$) such that $\Delta(\nu_{8a} - \nu_{7a}) > 90$ cm^{-1} and the intensity ratio $I(\nu_{8a})/I(\nu_{7a}) > 1$.[3]

Transition metal complexes employing Schiff base ligands are abundant in the literature owing to the ease of their synthesis and functionalization.[16] Foremost, they are utilized in many catalytic applications, such as polymerization, epoxidation, hydroxylation, and small molecule oxidation or reduction. Despite their abundance, the redox chemistry of Schiff base ligands is limited to salen-type complexes.[17] Several studies have concluded that one-electron oxidation of Ni^{II}(salen) is ligand-based, producing either a Ni^{II}−phenoxyl radical species that can polymerize,[18] or more commonly a Ni^{III}−phenolato complex ligated by a coordinating solvent.[19] Recently, Yamauchi et al. synthesized group 10 complexes of tbu-salen and tbu-salcn, where tbu-salen = *N*,*N*′-bis(3,5-di-*tert*-butylsalicylidene)ethylenediamine(2-) and tbu-salcn = *N*,*N*′-bis(3,5-di-*tert*-butylsalicylidene)-1,2-cyclohexanediamine(2-), and analyzed their one-electron oxidized products.[20,21] The results identified an elegant temperature- and solvent-dependent redox tautomerism that was conveniently monitored by EPR. A one-electron oxidation of Ni^{II}(tbu-salen) produces a Ni^{III}−phenolato complex at <−120 °C and a Ni^{II}−phenoxyl species at >−100 °C in dichloromethane. One-electron oxidation of Pt^{II}(tbu-salen) produced a monocation with the same charge distribution as the nickel complex, while the palladium complex is exclusively Pd^{II}−phenoxyl. No radical complexes were isolated in coordinating solvents, in line with previous studies.

We have synthesized the salen-type ligand, 2-((*E*)-(2-mercaptophenylimino)-methyl)-4,6-di-*tert*-butylphenolato(2-), L^{2-}, with a tridentate N,O,S coordination sphere. While

Scheme 1. Ligands and Complexes

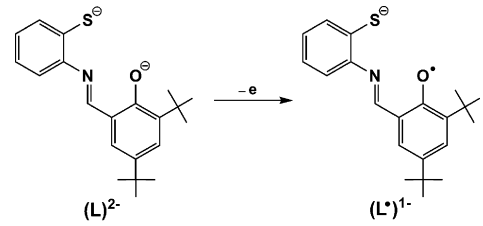

$[Fe^{III}(L\text{-}L)Br]$	S = 5/2	**1**
$[Ru^{III}_2(L)_2Cl_2(NCCH_3)_2]$	S = 0	**2**

variations of this Schiff base ligand have been complexed to transition metals previously,[22,23] the possibility of ligand redox has not been assessed. In this paper, the first of two successive papers, we will describe the synthesis and characterization of monomeric $[Fe^{III}(L-L)Br]^0$ (**1**) and dimeric $[Ru^{III}_2(L)_2Cl_2(NCCH_3)_2]^0$ (**2**) (Scheme 1), along with a spectroscopic and density functional theoretical examination of their oxidation products. Complex **1** is near identical to several previously reported iron complexes with N,O,S-donor Schiff base ligands and apical halides; however, only the structural parameters and room-temperature magnetic moments have been presented.[24,25] In the second part (Roy, N.; Sproules, S.; Bothe, E.; Weyhermüller, T.; Wieghardt, K. submitted), we will discuss the formation and rich redox chemistry of polynuclear compounds of L^{2-} with cobalt(III), copper(II), palladium(II), and platinum(II).

Experimental Section

Materials. All air-sensitive materials were manipulated using standard Schlenk line techniques or a glovebox. 3,5-Di-*tert*-butylsalicaldehyde was purchased from Aldrich and used as received. $FeBr_2$ and $RuCl_3 \cdot H_2O$ were purchased from Strem and used without further purificaton.

Synthesis of the Ligand. Synthesis of 2-((*E*)-(2-Mercaptophenylimino)methyl)-4,6-di-*tert*-butylphenol (H_2L). A solution of 3,5-di-*tert*-butylsalicyldehyde (3.74 g; 16.0 mmol) in dry methanol (30 mL) was treated dropwise with dry 2-aminothiophenol (2.00 g; 16.0 mmol). The reaction mixture was refluxed under argon for three hours. After cooling to room temperature, a yellow crystalline product was isolated by filtration and dried in the air. Yield: 4.5 g (82%).

H_2(L). Anal. calcd for $C_{21}H_{27}NOS$: C, 73.86; H, 7.96; N, 4.10; S, 9.38. Found: C, 73.72; H, 8.12; N, 4.16; S, 9.46. ^{1}H NMR (500 MHz, $CDCl_3$): δ 1.32 (s, 9H), 1.43 (s, 9H), 3.2 (s, 1H), 4.6 (s, 1H) 7.06−7.34 (m, 6H), 8.2 (s, 1H). EI mass spectrum: *m*/*z* 341 $[M]^+$.

Single crystals of its oxidized, disulfide-bridged dimeric form, H_2(L−L), were obtained by slow evaporation of a methanol solution in the air.

H_2(L−L). ^{1}H NMR (500 MHz, $CDCl_3$): δ 1.28 (s, 18H), 1.38 (s, 9H), 5.2 (s, 1H), 7.04−7.46 (m, 12H), 8.4 (s, 2H). EI mass spectrum: *m*/*z* 680 $[M]^+$.

(11) Sokolowski, A.; Adam, B.; Weyhermüller, T.; Kikuchi, A.; Hildenbrand, K.; Schnepf, R.; Hildebrandt, P.; Bill, E.; Wieghardt, K. *Inorg. Chem.* **1997**, *38*, 3702.
(12) Sokolowski, A.; Müller, J.; Weyhermüller, T.; Schnepf, R.; Hildebrandt, P.; Hildenbrand, K.; Bothe, E.; Wieghardt, K. *J. Am. Chem. Soc.* **1997**, *119*, 8889.
(13) Müller, E.; Rieker, A.; Scheffler, K.; Moosmayer, A. *Angew. Chem., Int. Ed.* **1966**, *5*, 6.
(14) Benisvy, L.; Bittl, R.; Bothe, E.; Garner, C. D.; McMaster, J.; Ross, S.; Teutloff, C.; Neese, F. *Angew. Chem., Int. Ed.* **2005**, *44*, 5314.
(15) Bill, E.; Müller, J.; Weyhermüller, T.; Wieghardt, K. *Inorg. Chem.* **1999**, *38*, 5795.
(16) Holm, R. H.; Everett, G. W.; Chakravorty, A. *Prog. Inorg. Chem.* **1966**, *7*, 83.
(17) (a) Kapturkiewicz, A.; Behr, B. *Inorg. Chim. Acta* **1983**, *69*, 247. (b) Zanello, P.; Cinquantini, A. *Trans. Met. Chem.* **1985**, *10*, 370.
(18) (a) de Castro, B.; Freire, C. *Inorg. Chem.* **1990**, *29*, 5113. (b) Vilas-Boas, M.; Freire, C.; de Castro, B.; Christensen, P. A.; Hillman, A. R. *Inorg. Chem.* **1997**, *16*, 4919.
(19) (a) de Castro, B.; Freire, C.; Pereira, E. *J. Chem. Soc., Dalton Trans.* **1994**, 571. (b) Freire, C.; de Castro, B. *J. Chem. Soc., Dalton Trans.* **1998**, 1491. (c) Carrondo, M. A. A. F. de C. T.; de Castro, B.; Coelho, A. M.; Domingues, D.; Freire, C.; Morais, J. *Inorg. Chim. Acta* **1993**, *205*, 157. (d) Goldsby, K. A.; Blaho, J. K.; Hoferkamp, L. A. *Polyhedron* **1989**, *8*, 113. (e) Azevedo, F.; Carrondo, M. A. A. F. de C. T.; de Castro, B.; Convery, M.; Domingues, D.; Freire, C.; Duarte, M. T.; Nielsen, K.; Santos, I. C. *Inorg. Chim. Acta* **1994**, *219*, 43.
(20) Shimazaki, Y.; Tani, F.; Fukui, K.; Naruta, Y.; Yamauchi, O. *J. Am. Chem. Soc.* **2003**, *125*, 10512.
(21) Shimazaki, Y.; Yajima, T.; Tani, F.; Karasawa, S.; Fukui, K.; Naruta, Y.; Yamauchi, O. *J. Am. Chem. Soc.* **2007**, *129*, 2559.
(22) (a) Kabak, M.; Elerman, Y.; Özbey, S.; Atakol, O. *J. Chem. Cryst.* **1995**, *25*, 259. (b) Labisbal, E.; De Blas, A.; García-Vázquez, J. A.; Romero, J.; Durán, M. I.; Sousa, A. *Polyhedron* **1992**, *11*, 227. (c) Wang, C.; Ma, Z.; Sun, X.-L.; Gao, Y.; Guo, Y.-H.; Tang, Y.; Shi, L.-P. *Organometallics* **2006**, *25*, 3259.
(23) Rajsekhar, G.; Rao, C. P.; Saarenketo, P. K.; Kolehmainen, E.; Rissanen, K. *Inorg. Chem. Commun.* **2002**, *5*, 649.
(24) Bertrand, J. A.; Breece, J. L. *Inorg. Chim. Acta* **1974**, *8*, 267.
(25) (a) Elmali, A.; Elerman, Y. *Acta Crystallogr., Sect. C.* **2001**, *57*, 375. (b) Elmali, A.; Elerman, Y. *Anal. Sci.* **2002**, *18*, 1399.

Synthesis of Complexes. [Fe^{III}(L−L)Br] (1). To a solution of H_2L (200 mg; 0.58 mmol) in acetonitrile (40 mL) was added $FeBr_2$ (126 mg; 0.58 mmol), which was then stirred under Ar for 10 min. Triethylamine (0.10 mL; 0.72 mmol) was introduced, and the reaction mixture was initially stirred under an Ar atmosphere for 30 min before it was exposed to the atmosphere and stirred for a further hour. The resultant dark red brown solution was filtered, and the green-brown microcrystalline product was collected by filtration and dried in vacuo. Black-green single crystals suitable for X-ray diffraction were obtained by slow evaporation of a 1:1 acetonitrile/hexane solution of the complex. Yield: 0.21 g (89% based on L).

Anal. calcd for $C_{42}H_{50}N_2O_2S_2BrFe$: C, 61.96; H, 6.18; N, 3.43; Fe, 6.87. Found: C, 61.56; H, 6.33; N, 3.21; Fe, 7.06. Electrospray ionization (ESI) mass spectrum (CH_2Cl_2, neg. ion mode): *m*/*z* 893.85 $[M + Br]^-$.

[Ru^{III}_2(L)$_2$Cl$_2$(NCCH$_3$)$_2$] (2). A pale yellow solution of H_2L (400 mg; 1.17 mmol) in acetonitrile (40 mL) was treated with $RuCl_3 \cdot H_2O$ (244 mg; 1.17 mmol). After 10 min of stirring under Ar, triethylamine (0.10 mL; 0.72 mmol) was added via syringe, and the reaction mixture was stirred for another 30 min under Ar. Afterwards, it was exposed to the atmosphere and stirred for an additional 2 h, generating a dark green-brown solution. This solution was filtered where after the microcrystalline solid formed was collected via filtration from the filtrate and dried in vacuo. Single crystals suitable for X-ray diffraction were grown by slow evaporation of a 1:1 acetonitrile/dichloromethane solvent mixture. Yield: 0.53 g (96%).

Anal. calcd for $C_{46}H_{56}N_4O_2S_2Cl_2Ru_2$: C, 53.42; H, 5.46; N, 5.41; Ru, 19.54. Found: C, 53.58; H, 5.57; N, 5.53; Ru, 19.6. ESI mass spectrum (CH_2Cl_2, pos. ion mode): *m*/*z* 952 $[M + H - 2CH_3CN]^+$.

Calculations. All DFT calculations were performed with ORCA.[26] Complex **1**, and its oxidized derivative, $[\mathbf{1}]^+$, were geometry optimized using the B3LYP functional.[27] The all-electron basis sets were those reported by the Ahlrichs' group.[28,29] Triple-ζ-quality basis sets with one set of polarization functions (TZVP) were used for all non-carbon and non-hydrogen atoms. The carbon and hydrogen atoms were described by slightly smaller polarized split-valence SV(P) basis sets that are double-ζ-quality in the valence region and contain a polarizing set of d functions on the non-hydrogen atoms.[28] Auxiliary basis sets used to expand the electron density in the calculations were chosen to match the orbital basis. Mössbauer spectral parameters have been calculated as previously described.[30] Geometry optimization of **2** and its oxidized derivatives, $[\mathbf{2}]^+$ and $[\mathbf{2}]^{2+}$, were carried out at the BP86 level of DFT.[31] A TZV(P) basis set was employed for ruthenium while smaller SV(P) basis sets were used for the remaining atoms. Again, auxiliary basis sets were chosen to match the orbital basis. Electronic energies and properties were calculated at the optimized geometries with the B3LYP functional.[27] Here, TZV(P) basis sets were used to describe all non-carbon and non-hydrogen atoms, with SV(P) basis sets used for carbon and hydrogen. The self-consistent field calculations were tightly converged (1×10^{-8} E_h in energy, 1×10^{-7} E_h in the density charge, and 1×10^{-7} in the maximum element of the DIIS[32] error vector). The geometry search for all complexes was carried out in redundant internal coordinates without imposing geometry constraints. Corresponding[33] and quasi-restricted[34] orbitals and density plots were obtained using Molekel.[35] We describe our computational results for $[\mathbf{1}]^+$ and $[\mathbf{2}]^{2+}$ using the broken-symmetry (BS) formulism.[30,36]

X-Ray Crystallographic Data Collection and Refinement of the Structures. Single crystals of H_2(L−L), **1**, and **2** were coated with perfluoropolyether, picked up with nylon loops, and immediately mounted in the nitrogen cold stream of a Bruker-Nonius KappaCCD diffractometer equipped with a Mo-target rotating-anode X-ray source. Graphite monochromated Mo Kα radiation (λ = 0.71073 Å) was used throughout. Final cell constants were obtained from least-squares fits of all measured reflections. Intensity data of **1** were corrected for absorption using intensities of redundant reflections using SADABS.[37] The data sets of compound **2** were corrected with the Gaussian-type absorption correction method embedded in XPREP.[38] The structures were readily solved by Patterson methods and subsequent difference Fourier techniques. The Siemens ShelXTL[38] software package was used for solution and artwork of the structures; ShelXL97[39] was used for the refinement. All non-hydrogen atoms were anisotropically refined, and hydrogen atoms were placed at calculated positions and refined as riding atoms with isotropic displacement parameters, except for some methyl-hydrogen atoms in disordered acetonitrile molecules of crystallization, which could not be reliably located. Crystallographic data of the compounds are listed in Table 1.

Physical Measurements. The equipment used for the temperature-dependent magnetic susceptibility data and Mössbauer spectroscopy has been described in ref 7. Cyclic and square-wave voltammograms were recorded with an EG&G potentiostat/galvanostat in CH_2Cl_2 solutions (0.10 M $[N(n\text{-}Bu)_4]PF_6$) at a glassy carbon working electrode. Ferrocene was used as an internal standard; all redox potentials are given versus the ferrocenium/ferrocene (Fc^+/Fc) couple. Electronic absorption spectra were obtained using a Perkin-Elmer Lambda 19 spectrophotometer (200−2000 nm). Spectroelectrochemical measurements employed a Hewlett-Packard HP 8452A diode array spectrophotometer (200−1100 nm). X-band EPR spectra were recorded on a Bruker ESP 300 spectrometer and simulated using ESIM developed by Dr. E. Bill. NMR spectra were recorded on a Varian 500 MHz instrument at ambient temperature. Element analyses were performed by H. Kolbe at the Mikroanalytisches Laboratorium in Mülheim an der Ruhr, Germany.

(26) Neese, F. *Orca*, version 2.6, revision 35; Universität Bonn: Bonn, Germany, 2008.
(27) (a) Becke, A. D. *J. Chem. Phys.* **1993**, *98*, 5648. (b) Lee, C. T.; Yang, W. T.; Parr, R. G. *Phys. Rev. B: Condens. Matter Mater. Phys.* **1988**, *37*, 785.
(28) Schäfer, A.; Horn, H.; Ahlrichs, R. *J. Chem. Phys.* **1992**, *97*, 2571.
(29) Schäfer, A.; Huber, C.; Ahlrichs, R. *J. Chem. Phys.* **1994**, *100*, 5829.
(30) Roy, N.; Sproules, S.; Bill, E.; Weyhermüller, T.; Wieghardt, K. *Inorg. Chem.* **2008**, *47*, 10911.
(31) (a) Becke, A. D. *J. Chem. Phys.* **1986**, *84*, 4524. (b) Perdew, J. P. *Phys. Rev. B: Condens. Matter Mater. Phys.* **1986**, *33*, 8822.
(32) (a) Pulay, P. *Chem. Phys. Lett.* **1980**, *73*, 393. (b) Pulay, P. *J. Comput. Chem.* **1992**, *3*, 556.
(33) Neese, F. *J. Phys. Chem. Solids* **2004**, *65*, 781.
(34) Schöneboon, J. C.; Neese, F.; Thiele, W. *J. Am. Chem. Soc.* **2005**, *127*, 5840.
(35) Molekel, Advanced Interactive 3D-Graphics for Molecular Sciences, Swiss National Supercomputing Center. http://www.cscs.ch/molekel (accessed Feb 2009).
(36) (a) Noodleman, L. *J. Chem. Phys.* **1981**, *74*, 5737. (b) Noodleman, L.; Case, D. A.; Aizman, A. *J. Am. Chem. Soc.* **1988**, *110*, 1001. (c) Noodleman, L.; Davidson, E. R. *Chem. Phys.* **1986**, *109*, 131. (d) Noodleman, L.; Norman, J. G.; Osborne, J. H.; Aizman, A.; Case, D. A. *J. Am. Chem. Soc.* **1985**, *107*, 3418. (e) Noodleman, L.; Peng, C. Y.; Case, D. A.; Monesca, J. M. *Coord. Chem. Rev.* **1995**, *144*, 199.
(37) *SADABS*, version 2006/1; Sheldrick, G. M., Ed.; Universität Göttingen: Göttingen, Germany, 2006.
(38) *ShelXTL 6.14*; Bruker AXS Inc.: Madison, WI, 2003.
(39) *ShelXL97*; Sheldrick, G. M., Ed.; Universität Göttingen: Göttingen, Germany, 1997.

Table 1. Crystallographic Data for H_2(L−L), **1**, and **2**·4 MeCN

	H_2(L−L)	**1**	**2**·4 MeCN
chem. formula	$C_{42}H_{52}N_2O_2S_2$	$C_{42}H_{50}BrFeN_2O_2S_2$	$C_{54}H_{68}Cl_2N_8O_2Ru_2S_2$
fw	680.98	814.72	1198.32
space group	C_2, No. 5	$P\bar{1}$, No. 2	$P\bar{1}$, No. 2
A, Å	19.5412(8)	9.5168(2)	9.6523(3)
B, Å	6.3313(3)	12.0611(3)	10.2887(3)
C, Å	15.5369(6)	18.5063(5)	14.3769(5)
α, deg	90.00	105.525(3)	98.765(3)
β, deg	98.288(4)	100.812(3)	91.933(3)
γ, deg	90.00	90.288(3)	97.159(3)
V, Å	1902.17(14)	2006.94(8)	1398.06(8)
Z	2	2	1
T, K	100(2)	100(2)	100(2)
ρ calcd, g cm^{-3}	1.189	1.348	1.423
reflns collected/2Θ$_{max}$	24018/65.00	61081/65.00	45848/67.00
unique reflns/$I > 2\sigma(I)$	6702/6561	14438/13574	10838/10461
no. of params/restraints	226/ 1	463/0	325/0
λ, Å/*μ*(Kα), cm^{-1}	0.71073/15.12	0.71073/15.12	0.71073/7.57
R1[a]/goodness of fit[b]	0.0293/ 1.059	0.0279/1.104	0.0191/1.069
wR2[c] ($I > 2\sigma$ (I))	0.0757	0.0691	0.0462
residual density, eÅ^{-3}	+0.28/−0.15	+0.51/−0.38	+0.50/−0.60

[a] Observation criterion: $I > 2\sum(I)$. $R1 = \sum||F_o| - |F_c||F_o|$, [b] $GoF = [\sum[w(F_o^2 - F_c^2)^2]/(n - p)]^{1/2}$. [c] $wR2 = [\sum[w(F_o^2 - F_c^2)^2]/\sum[w(F_o^2)^2]]^{1/2}$ where $w = 1/\sigma^2(F_o^2) + (aP)^2 + bP$, $P = (F_o^2+2F_c^2)/3$.

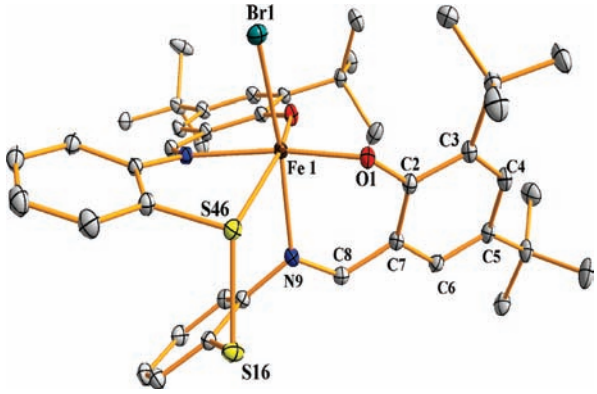

Figure 1. Perspective view of the neutral molecule in crystals of **1**.

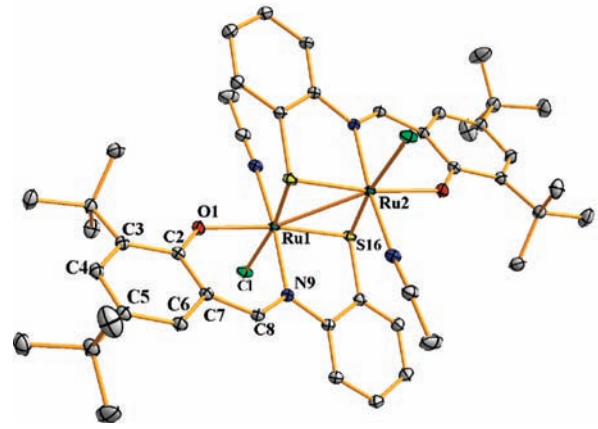

Figure 2. Structure of the neutral molecule in crystals of **2**.

Results

Synthesis and X-ray Structures. The tridentate N,O,S-donor ligand 2-(*E*)-(2-mercaptophenyl)-4,6-di-*tert*-butylphenol (H_2L) is produced from the condensation of 3,5-di-*tert*-butylsalicylaldehyde with 2-aminothiophenol. Its dimeric form, H_2(L−L), was obtained by slow evaporation of a methanol solution of the deprotonated ligand in the air. The reaction of equimolar amounts of $FeBr_2$ and H_2L in the presence of NEt_3 did not produce the desired dimer analogous to **2**. Instead, the stable mononuclear complex [Fe^{III}-(L−L)Br]^0 (**1**) was obtained. A near identical complex was isolated previously by Bertrand et al.; however, here they combined equimolar amounts of the disulfide-bridged ligand dimer, $(L-L)^{2-}$, with $FeCl_3$.[24] The crystal structure of **1** contains a ferric ion coordinated by this pentadentate N_2O_2S-donor ligand, $(L-L)^{2-}$ (Figure 1). The sixth coordination site is occupied by a Br ligand. The Fe ion rests 0.116 Å out of the NO_2S equatorial plane, while the Br(1)−Fe−N(9), O(1)−Fe−N(39), and O(31)−Fe−S(46) angles of 172.34(4)°, 163.65(3)°, and 162.47(3)°, respectively, highlight the degree of distortion from octahedral geometry. The Fe−O and Fe−N distances at 1.8974(9), 1.9073(8), 2.1515(10), and 2.1665(10) Å, respectively, are similar to previously reported Fe^{III} complexes with Schiff base ligands,[24,25] and the Fe−Br bond length of 2.4804(2) Å is unremarkable. The S−S distance of 2.0827(4) Å and the long Fe−S distance of 2.6210(3) Å are typical of the Fe−S−S moiety in the near-identical chloro(bis{salicylideniminephenyl}-disulfide)iron(III), containing the same sulfide-bridged ligand sans ^{t}Bu substituents.[24] The disulfide formation is caused by aerial oxidation, as is shown to occur with the deprotonated ligand, H_2(L−L).

The ruthenium salt, $RuCl_3 \cdot H_2O$, reacts with an equimolar amount of H_2L, to afford a neutral, dimeric complex, [Ru_2(L)$_2Cl_2$(NCCH$_3$)$_2$]^0 (**2**). Each six-coordinated ruthenium center bound to one ligand L^{2-}, the sulfur-donor atom of the second L^{2-} ligand, one chloride, and one molecule of solvent, acetonitrile (Figure 2). The two edge-sharing octahedra are related by a crystallographic axis of symmetry. The O(1)−Ru(1)−S(16), N(9)−Ru(1)−N(41), and Cl(31)−Ru(1)−S(16″) angles of 169.27(2)°, 170.041(8)°, and 172.89(3)°, respectively, underscore the slight distortion in the octahedra, and the Ru atom lies 0.158 Å above the N_2OS equatorial plane. The Ru−O, Ru−N, and Ru−Cl bond distances are typical for Ru^{III} complexes. The two metal centers are bridged by the sulfur atoms of L^{2-}, producing a planar Ru_2S_2 diamond core with Ru−S distances averaging 2.29 Å and an acute Ru−S−Ru angle of 75.655(7)° and

Table 2. Intraligand Bond Distances (Å) for H_2(L−L), **1**, and **2**

	H_2(L−L)	**1**	**2**
O(1)−C(2)	1.348(1)	1.320(1)	1.310(1)
C(2)−C(7)	1.408(1)	1.419(2)	1.428(1)
C(2)−C(3)	1.407(1)	1.432(2)	1.436(1)
C(3)−C(4)	1.391(1)	1.390(1)	1.390(1)
C(4)−C(5)	1.406(1)	1.412(2)	1.416(1)
C(5)−C(6)	1.378(1)	1.375(2)	1.378(1)
C(6)−C(7)	1.403(1)	1.414(2)	1.416(1)
C(7)−C(8)	1.444(1)	1.437(2)	1.439(1)
C(8)−N(9)	1.286(1)	1.298(2)	1.304(1)
N(9)−C(10)	1.408(1)	1.426(1)	1.432(1)
C(10)−C(15)	1.401(1)	1.405(2)	1.405(1)
C(10)−C(11)	1.391(1)	1.392(2)	1.399(1)
C(11)−C(12)	1.387(1)	1.392(2)	1.396(1)
C(12)−C(13)	1.392(1)	1.392(2)	1.390(1)
C(13)−C(14)	1.389(1)	1.393(2)	1.394(1)
C(14)−C(15)	1.387(1)	1.395(2)	1.393(1)
C(15)−S(16)	1.774(1)	1.767(1)	1.7784(8)
S(16)−S(46)	2.0214(4)	2.0827(4)	

obtuse S−Ru−S angle of 104.344(7)°. This affords a S···S distance of 3.618 Å and the short metal−metal distance of 2.8091(2) Å, which represents a Ru−Ru single bond. A similar arrangement is shown in the structures of $[Ru^{III}(H_2edta)(\mu\text{-}SC_6H_5)]_2$,[40] $[Ru^{III}_2(pyN_2H_2S_2)_2]^{2+}$,[41] and a number of $[Cp^*Ru(\mu\text{-}SR)]_2$ (R = alkyl or aryl)[42] complexes exhibiting Ru^{III}−Ru^{III} single bonds ranging from 2.7 to 2.9 Å.

The intraligand bond distances in complexes **1** and **2** are interesting in that the C−O bond length is somewhat short for a phenolato moiety, though longer than a $C-O_{phenoxyl}$ (1.26−1.29 Å) previously reported.[4−6] The intraligand bond distances for H_2(L−L), **1**, and **2** are listed in Table 2. Our reference point is the crystallographically characterized ligand dimer, H_2(L−L) (Figure S1, Supporting Information). It possesses a crystallographic center of symmetry, and it is stabilized by intramolecular hydrogen bonds of the type N···H−O in the salen unit. As in **1**, the two ligand units connect through the formation of a S−S bond of 2.0214(4) Å. The C(2)−O(1) and C(15)−S(16) bond lengths of 1.348(1) and 1.774(1) Å, respectively, are typical of single bonds. The C(8)−N(9) distance of 1.286(1) Å is indicative of a double bond, while the N(9)−C(10) distance is considerably longer at 1.408(1) Å. Both the phenolate and aminothiophenolate aromatic rings possess equidistant C−C bond distances within experimental error at ∼1.39−1.40 Å.

There are several reported structures of dimerized ligands of this type, bridged through a disulfide bond, as well as sulfur-methylated monomeric moieties, with various substitution patterns.[43] All of these ligand structures possess the same intraligand bond distance pattern as identified for H_2(L−L). Additionally, the structure is quite similar to a related salen-type ligand, 1,2-di-(*o*-salicyaldiminophenylthio)ethane, where an ethane bridge links the two N,O,S halves of the hexadentate ligand.[23] In contrast, complexing L^{2-} to a metal ion produces a decrease in the C−O bond length of 0.028 Å in **1** and 0.038 Å in **2**.

Scheme 2. Resonance Structures **A** and **B** of L^{2-}

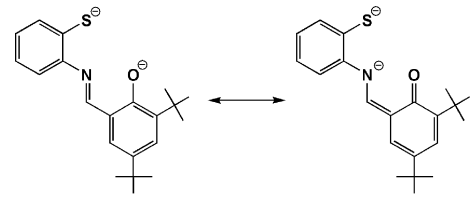

Furthermore, the phenolate C−C bond distances become more inequivalent, with C(3)−C(4) and C(5)−C(6) shorter than the other four C−C bonds. Additionally, the C═N is slightly lengthened. The bond distances within the aminothiophenolate portion of L^{2-} remain unchanged across the three structures. A short C−O distance of 1.32(1) Å was seen in chloro(bis{salicylideniminephenyl}disulfido)iron(III), and the intraligand bond pattern is identical to that in **1** and **2**.[24] The observed quinoidal-type distortion of the phenolate arm is accounted for by examining two resonance forms of L^{2-} (Scheme 2). However, given the considerable double bond character in the C−N bond in each of the structures, we can attribute a greater weight to canonical form **A**.

Many crystallographically characterized complexes containing variations of this N,O,S-donor Schiff base-type ligand exhibit this semiquinoidal distortion;[22,24,25,44] however, there has to our knowledge been no mention of the resonance forms that account for the structural outcome.

Electrochemistry and EPR Spectroscopy. The ferric center in **1** is high-spin, as denoted by its temperature-independent μ_{eff} value of 5.9 μ_B (Figure 3). It afforded a rhombic EPR spectrum that is characteristic of high-spin Fe^{III}, with a low-field feature at $g' = 9.5$ from the lowest Kramer's doublet, $m_s = \pm^5/_2$, and three g values from the $m_s = \pm^3/_2$ Kramer's doublet at $g' = 4.3$ (inset, Figure 3). Simulation was accomplished with $g_x = 2.00$, $g_y = 1.97$, and $g_z = 2.05$; a zero-field splitting of 3.5 cm^{-1}; and a rhombicity of 0.285. The line shape of the $g' = 4.3$ portion of the spectrum was realized using a Gaussian distribution of *E*/*D* with a half-width $\sigma = 0.035$.

The Mössbauer parameters ($\delta = 0.51$ mm s^{-1}; $|\Delta E_Q| = 0.81$ mm s^{-1}) are clearly indicative of a high-spin ferric ion

(40) Cameron, B. R.; Bridger, G. J.; Maresca, K. P.; Zubieta, J. *Inorg. Chem.* **2000**, *39*, 3928.
(41) Sellmann, D.; Shaban, S. Y.; Rösler, A.; Heinemann, F. W. *Inorg. Chim. Acta* **2005**, *358*, 1798.
(42) (a) Kondo, T.; Uenoyama, S.; Fujita, K.; Mitsudo, T. *J. Am. Chem. Soc.* **1999**, *121*, 482. (b) Takahashi, A.; Mizobe, Y.; Tanase, T.; Hidai, M. *J. Organomet. Chem.* **1995**, *496*, 109. (c) Hidai, M.; Imagawa, K.; Cheng, G.; Mizobe, Y.; Wakatsuki, Y.; Yamazaki, H. *Chem. Lett.* **1986**, 1299. (d) Dev, S.; Imagawa, K.; Mizobe, Y.; Cheng, G.; Wakatsuki, Y.; Yamazaki, H.; Hidai, M. *Organometallics* **1989**, *8*, 1232. (e) Matsuzaka, H.; Hirayama, Y.; Nishio, M.; Mizobe, Y.; Hidai, M. *Organometallics* **1993**, *12*, 36. (f) Onodera, G.; Matsumoto, H.; Nishibayashi, Y.; Uemura, S. *Organometallics* **2005**, *24*, 5799. (g) Becker, E.; Mereiter, K.; Schmid, R.; Kirchner, K. *Organometallics* **2004**, *23*, 2876.
(43) (a) Jin, L.-X.; Liu, Z.; Xia, J.-L.; Li, G.-Z. *Acta Crystallogr., Sect. E.* **2007**, *E63*, o3854. (b) Ancin, N.; Çelik, O.; Öztaş, S. G.; İde, S. *Struct. Chem.* **2007**, *18*, 347. (c) Hamaker, C. G.; Corgliano, D. M. *Acta Crystallogr., Sect. E.* **2006**, *62*, o3354. (d) Hamaker, C. G.; Corgliano, D. M. *Acta Crystallogr., Sect. E.* **2006**, *E62*, o3354. (e) Wang, D.; Behrens, A.; Farahbakhsh, M.; Gatjens, J.; Rehder, R. *Chem.—Eur. J.* **2003**, *9*, 1805. (f) Ruiz-Pérez, C.; González-Platas, J.; Rodríguez-Romero, F. V. *Acta Crystallogr., Sect. C.* **1995**, 1016–C51. (g) Elmali, A.; Özbey, S.; Kendi, E.; Kabak, M.; Elerman, Y. *Acta Crystallogr., Sect. C.* **1995**, *C51*, 1878.
(44) (a) Elerman, Y.; Kabak, M.; Svoboda, I. *J. Chem. Cryst.* **1996**, *26*, 29. (b) Hahn, R.; Herrmann, W. A.; Artus, G. R. J.; Kleine, M. *Polyhedron* **1995**, *14*, 2953.

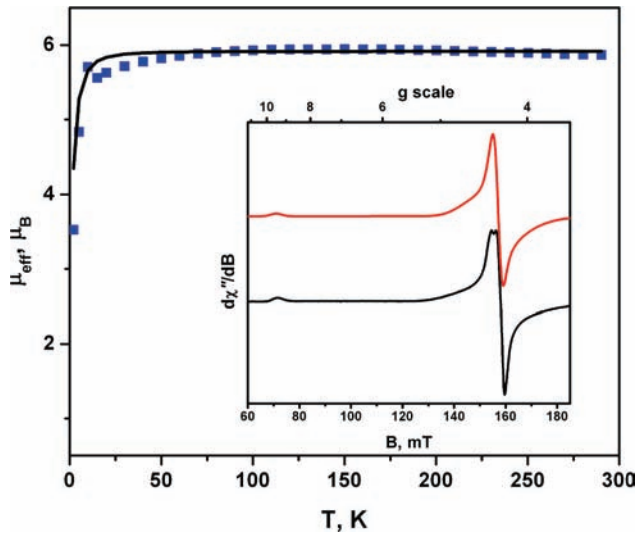

Figure 3. Temperature-dependence of the effective magnetic moment, μ_{eff}, μ_B, of a solid sample of **1**. Filled squares represent the experimental data; the solid line is a best fit with $S = {}^5/_2$, $g = 2.01$, $D = 3.5$ cm^{-1}, and $E/D = 0.285$ (fixed from EPR). Inset: EPR spectrum of **1** in CH_2Cl_2/toluene at 10 K. Experimental conditions: frequency, 9.43 GHz; power, 0.63 mW; modulation, 1.0 mT. Red: simulation (see text). Black: Experimental spectrum.

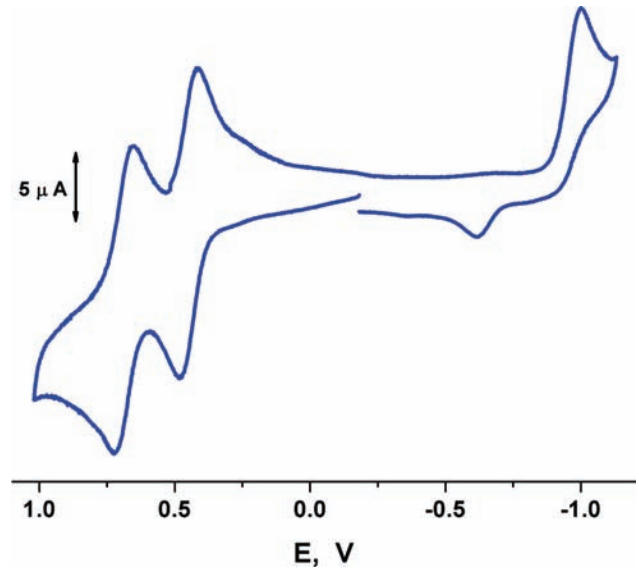

Figure 4. CV of **2** in CH_2Cl_2 containing 0.10 M [N(*n*-Bu)$_4$]PF_6 as the supporting electrolyte at 25 °C at a glassy carbon working electrode at a scan rate of 50 mV s^{-1}. Potentials are referenced versus Fc^+/Fc.

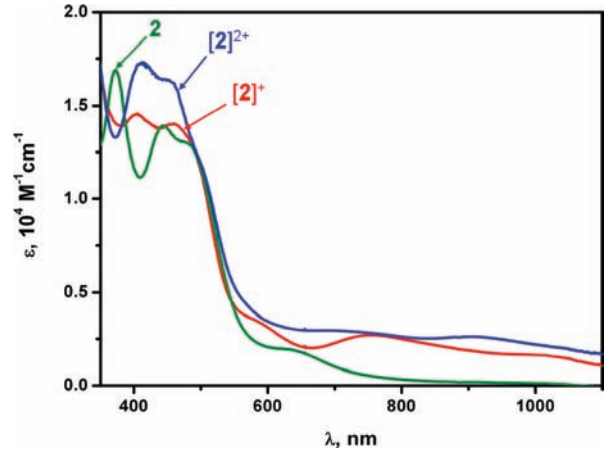

Figure 5. Electronic absorption spectra of **2** and of the coulometrically generated oxidized forms $[\mathbf{2}]^+$ and $[\mathbf{2}]^{2+}$ in CH_2Cl_2 containing 0.10 M [N(*n*-Bu)$_4$]PF_6 as the supporting electrolyte at −25 °C.

(Figure S2, Supporting Information). Its electronic absorption spectrum has an intense phenolato $\pi \rightarrow \pi^*$ transition at 372 nm ($\varepsilon = 1.34 \times 10^4$ M^{-1} cm^{-1}) and a phenolato → Fe charge transfer (CT) band at 624 nm (3200) (Figure S3, Supporting Information). The cyclic voltammogram (CV) of **1** shows two reversible and two irreversible processes (Figure S4, Supporting Information). The oxidation of **1** at +0.78 V is reversible on the CV time scale; however, controlled potential coulometric studies demonstrate that the oxidized species is too unstable for spectroelectrochemical analysis. DFT calculations prefer oxidation of the ligand rather than the formation of an Fe(IV) species. The reductive processes are suspected to arise from an irreversible reduction of the disulfide bridge and a reversible Fe^{III}/Fe^{II} couple at −1.7 V.

The two reversible oxidation processes observed at +0.45 and +0.69 V in the CV of **2** are both assigned as ligand-centered (Figure 4). An irreversible reduction presumably to a Ru(II/III) mixed valence species is seen at −1.0 V. The oxidation potentials are directly analogous to several known complexes in which one or more coordinated phenoxyl radicals are formed.[4,7,9,12,21] The electronic spectra of **2**, $[\mathbf{2}]^+$, and $[\mathbf{2}]^{2+}$ are overlaid in Figure 5 and display the classic hallmarks of phenoxyl coordination. Two intense UV bands at 373 (1.69×10^4) and 444 nm (1.39×10^4) are assigned as phenolate $\pi \rightarrow \pi^*$ transitions, with a shoulder at 618 nm (1980) attributed at a phenolato → Ru CT band.

Upon one- and two-electron oxidation of **2**, two broad, low-energy CT bands are exhibited in the near-IR region, at 755 (2700) and 1000 nm (1640) for $[\mathbf{2}]^+$ and 675 (2960) and 904 nm (2620) for $[\mathbf{2}]^{2+}$. Additionally, **2** has an absorption minimum at 405 nm, while both $[\mathbf{2}]^+$ and $[\mathbf{2}]^{2+}$ possess absorption maxima at 404 (1.45×10^4) and 412 nm (1.73×10^4), respectively. This fingerprint for phenoxyl radical coordination was observed in systems employing 1,4,7-triazacyclononane with pendant phenolate arms,[7,11,12] and similar coordination motifs.[5,8,9] Furthermore, the phenolato $\pi \rightarrow \pi^*$ transition at 380 nm diminishes upon oxidation.

Coulometric one-electron oxidation of **2** produces an $S = {}^1/_2$ species that was probed by EPR spectroscopy. The near-axial spectrum of $[\mathbf{2}]^+$ shown in Figure 6 has $g_1 = 2.028$, $g_2 = 2.025$, and $g_3 = 1.978$, consistent with the formation of a phenoxyl radical. There is no observable hyperfine despite the noted delocalization of the unpaired electron through the phenoxyl ring where proton superhyperfine features have previously been seen.[12,15] Moreover, the lack of ruthenium hyperfine (^{99,101}Ru, $I = {}^5/_2$, 29.7% natural abundance) may suggest that the phenoxyl radical is uncoordinated. However, the simulated linewidths (1.0, 1.1, and 1.8 mT) are larger than that for free phenoxyls (typically 1.0 mT), obscuring any hyperfine features. The large g anisotropy ($\Delta g = 0.050$), not present in the EPR spectrum of a free phenoxyl ($\Delta g = 0.004$),[14] is a consequence of spin−orbit coupling to the metal center ($\xi_{Ru} = 1180$

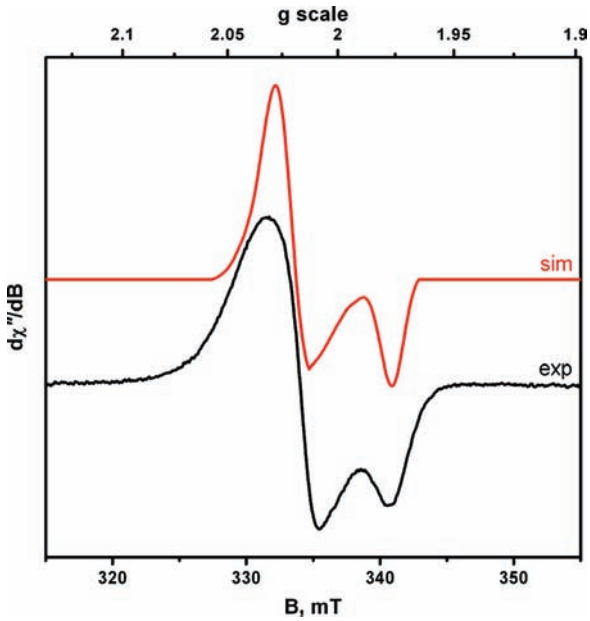

Figure 6. X-band EPR spectrum of coulometically generated $[\mathbf{2}]^+$ in CH_2Cl_2 at 10 K (conditions: frequency, 9.44 GHz; modulation, 1.0 mT; power, 0.10 mW).

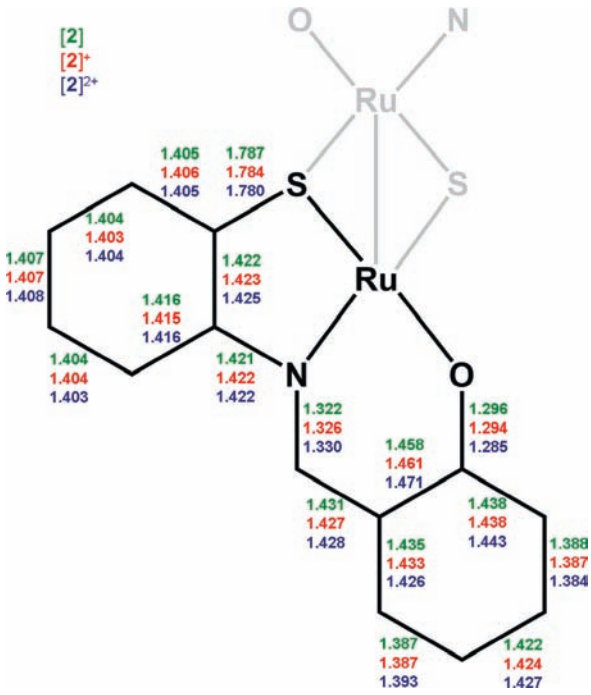

Figure 7. Calculated intraligand bond distances (Å) for **2**, $[\mathbf{2}]^+$, and $[\mathbf{2}]^{2+}$. For experimental values, see Table 2.

cm^{-1}),[13,45] such that $[\mathbf{2}]^+$ is formulated as $[Ru^{III}_2(L^{\bullet})(L)Cl_2(NCCH_3)_2]^+$ with a *coordinated* phenoxyl radical.

Calculations. A picture of the electronic structure of **1** was derived from DFT calculations using the B3LYP functional for the molecular orbital (MO) descriptions and spin distribution. The geometry of **1** was calculated spin-unrestricted ($S = {}^5/_2$) where the *tert*-butyl groups were truncated to decrease computation time. The geometry optimized molecular structure matches very closely with that

(45) Mabbs, F. E.; Collison, D. *Electron Paramagnetic Resonance of d Transition Metal Compounds*; Elsevier: Amsterdam, 1992.

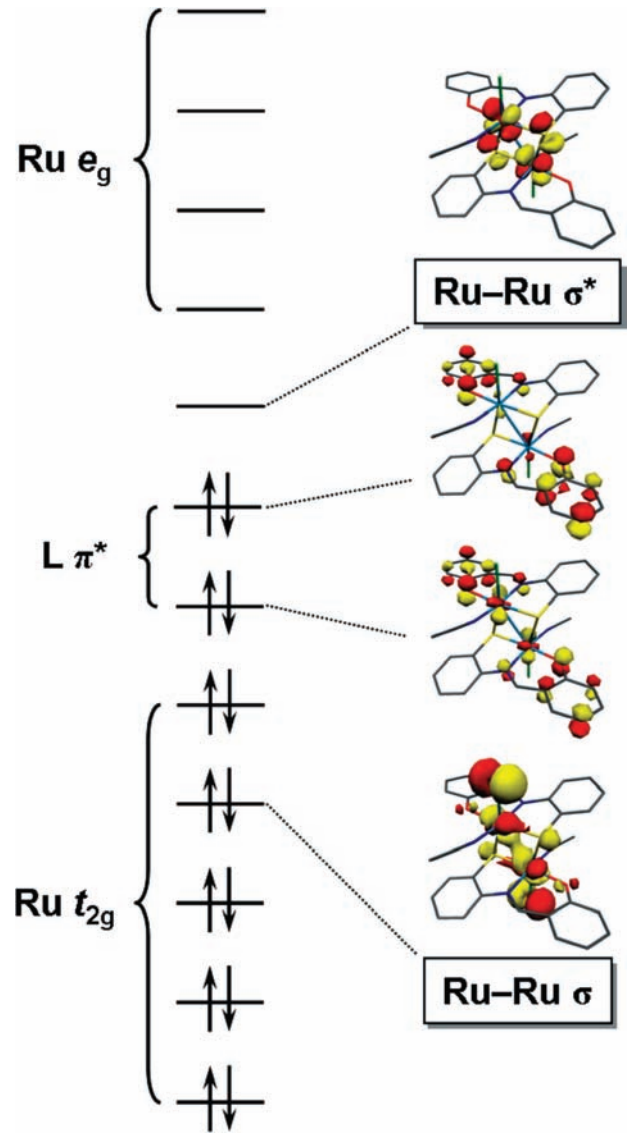

Figure 8. Qualitative MO scheme for neutral **2** ($S = 0$) as derived from a spin-unrestricted Kohn−Sham DFT calculation.

Table 3. Experimental and Calculated Bond Distances (Å) and Angles (deg) That Define the Ru_2S_2 Core in **2**, $[\mathbf{2}]^+$, and $[\mathbf{2}]^{2+}$

	exptl	calcd		
	2	**2**	$[\mathbf{2}]^+$	$[\mathbf{2}]^{2+}$
Ru(1)−S(16)	2.2688(2)	2.315	2.313	2.315
Ru(1)−S(46)	2.3112(2)	2.412	2.416	2.428
Ru(1)−S(16)−Ru(2)	75.655(7)	75.9	74.5	75.0
S(16)−Ru(1)−S(46)	104.344(7)	104.1	104.1	105.0
Ru(1)−Ru(2)	2.8091(2)	2.907	2.863	2.890
S(16)···S(46)	3.618	3.728	3.765	3.762

of the crystallographically characterized one. The intraligand bond distances are in excellent agreement with the experimental results. The calculated C−O and C−S bond lengths are within ±0.02 Å, while the remaining C−C and C−N distances are within ±0.01 Å. The metal−ligand distances are slightly overestimated, as has been observed before with this hybrid functional. Furthermore, the observed quinoidal distortion in the phenolate portion of the ligand was faithfully reproduced. The qualitative MO bonding scheme exhibits five singly occupied MOs (SOMOs) in the spin-up (α-spin) manifold with >75% Fe d character (see the Supporting

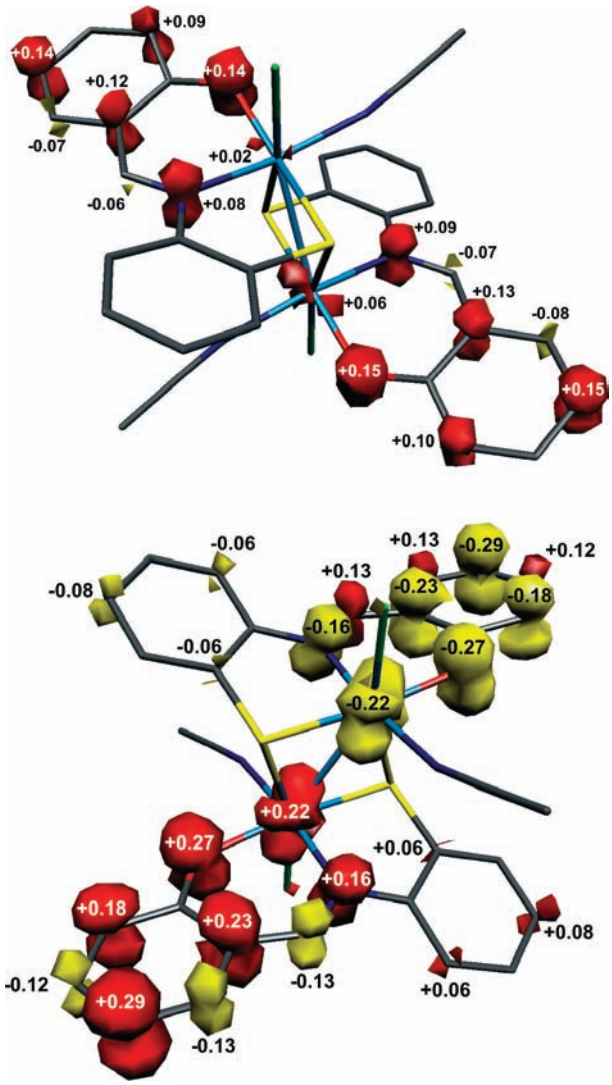

Figure 9. Spin density plots from Mulliken spin population analyses. Top, $[\mathbf{2}]^{+}$; bottom, $[\mathbf{2}]^{2+}$ (red, α-spin; yellow, β-spin).

Information). This is the hallmark of a high-spin Fe^{III} (d^5) ion. The Mulliken spin density analysis shows less than five unpaired electrons (4.1 spins) at the metal center resulting from the highly covalent metal−ligand bonds that distribute α-spin density onto each of the first coordination sphere donors (0.8 spins). Additionally, a calculated isomer shift, $\delta = 0.56$ mm s^{-1}, and quadrupole splitting, $\Delta E_Q = 0.83$ mm s^{-1}, for **1** are in excellent agreement with the experimental Mössbauer parameters ($\delta = 0.51$ mm s^{-1}; $|\Delta E_Q| = 0.81$ mm s^{-1}).

Its one-electron oxidized species, $[\mathbf{1}]^{+}$, was geometry optimized using a BS(5,1) $S = 2$ state. While there is no conclusive evidence for a ligand-centered oxidation of **1** given its short lifetime, the calculated structure portrays a high-spin ferric ion coordinated by an oxidized ligand, specifically the meridionally coordinated N,O,S portion of the pentadentate ligand (see the Supporting Information). This state is 9.1 kcal mol^{-1} more energetically favorable than the corresponding low-spin Fe^{III} $S = 0$ state.

The geometry optimization of truncated **2** was carried out using the BS(1,1) approach and the BP86 functional. The calculated metal−ligand and intraligand bond distances are

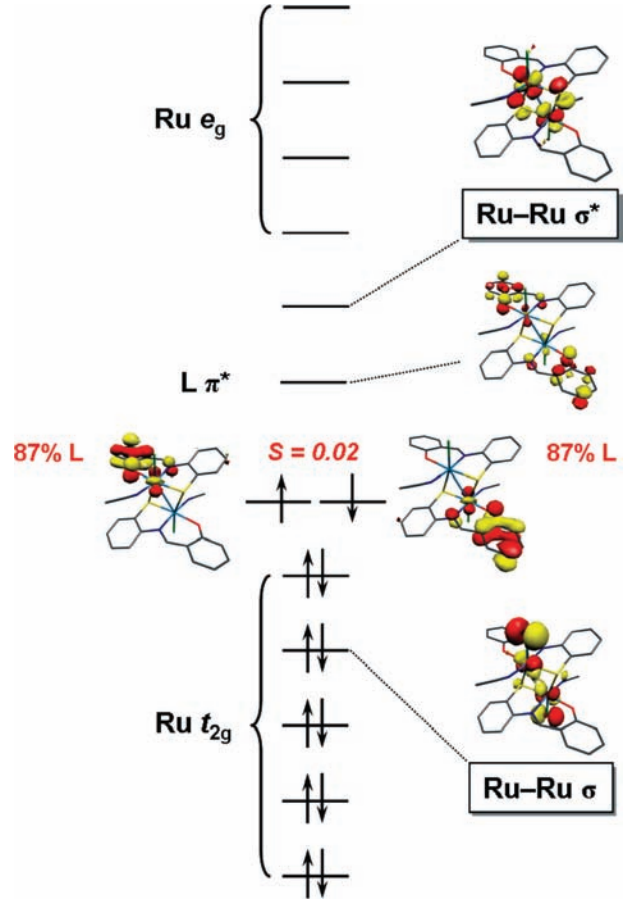

Figure 10. Qualitative MO scheme for dicationic $[\mathbf{2}]^{2+}$ ($S = 0$) as derived a from BS(1,1) DFT calculation.

in excellent agreement with experimental results (Figure 7). Particularly noteworthy is that the dimensions of the Ru_2S_2 diamond core are well-reproduced. The qualitative MO bonding scheme derived from a single-point calculation using the B3LYP functional identifies two d orbitals of each metal that are doubly occupied, while a singly occupied d_{xz} orbital overlaps to form a metal−metal σ bond (Figure 8). The LUMO is the antibonding Ru−Ru σ^*. The two highest occupied MOs are both ligand-based, specifically, a C−O π^* of the phenolate part of L^{2-}. The Ru e_g orbitals remain unoccupied; thus, the manifold clearly describes **2** as $[Ru^{III}_2(L)_2Cl_2(NCCH_3)_2]^0$. Hence, despite using the BS(1,1) approach, a broken symmetry solution was not obtained by virtue of the Ru−Ru single bond.

Geometry optimizations of singly and doubly oxidized $[\mathbf{2}]^{+}$ and $[\mathbf{2}]^{2+}$, respectively, were also performed using the BP86 functional. The reversibility of the oxidation processes suggests that there is no change in the ligand coordination number and type that the geometry optimized coordinates for **2** used as a starting point for its oxidized derivatives. Since there are no X-ray structures of $[\mathbf{2}]^{+}$ and $[\mathbf{2}]^{2+}$, we cannot compare the calculated metrical details; however, it is noteworthy to contrast the changes in the intraligand bond distances as dimer **2** is oxidized. As displayed in Figure 7, there is very little change in these bond distances, with the exception of a slightly more pronounced semiquinoidal distortion in the phenolate moiety. The dimensions of the

Ru_2S_2 core are identical such that the Ru−Ru σ bond is retained throughout the electron transfer series (Table 3).

The MO manifold for $[\mathbf{2}]^+$ shows a d orbital occupation consistent with two low-spin Ru^{III} ions and a phenolate π^* SOMO distributed symmetrically over both ligands. The Mulliken spin density analysis shows one α-spin dispersed over both ligands (Figure 9). For the phenolate ring, the typical alternating spin density distribution is obtained with a significant amount of positive spin population located at the O, C_{ortho}, and C_{para}atoms.

Furthermore, there is a significant amount of spin on the N, derived through conjugation with the phenolate ring, while no spin density is observed on the thiophenolate moiety. The miniscule amount of spin density located at the Ru centers is consistent with no experimentally observed metal hyperfine in the EPR spectrum. Thus, oxidation of **2** generates a phenoxyl radical complex, $[Ru^{III}_2(L^{\bullet})(L)Cl_2(NCCH_3)_2]^+$.

In $[\mathbf{2}]^{2+}$, a broken symmetry BS(1,1) solution is obtained with the MO manifold depicting a singlet diradical solution. The SOMOs are ligand-based (87%) phenoxyl radicals with a small orbital overlap integral of S = 0.02 (Figure 10). The Ru d orbital occupancy is consistent with two low-spin Ru^{III} ions. The Mulliken spin density plot shows one α-spin electron distributed over one ligand, while there is an equal amount of β-spin on the other $(L^{\bullet})^{1-}$ ligand (Figure 9). Again, there is an alternating pattern of positive and negative spin density throughout the phenolate rings of both ligands with large concentrations found at the O, C_{ortho}, C_{para}, and N atoms. Therefore, the doubly oxidized product of **2** is formulated as $[Ru^{III}_2(L^{\bullet})_2Cl_2(NCCH_3)_2]^{2+}$, a singlet diradical dication.

Conclusion

The tridentate N,O,S-donor ligand, L^{2-}, has been coordinated to iron and ruthenium, resulting in quite different compounds. Monomeric **1** containing a high-spin ferric ion ($S = {}^5/_2$) bound to a five-coordinate $(L-L)^{2-}$, a disulfide bridged ligand dimer. In contrast, ruthenium forms the dimeric **2** in which a $Ru^{III}-Ru^{III}$ single bond sits at its core. Most interestingly, this diamagnetic molecule can be reversibly one-electron oxidized twice, and these are ligand-centered redox processes. Although this N,O,S-donor ligand and its variants have been synthesized and characterized previously,[43] along with numerous metal complexes,[22,24,25,44] this is the first time that its redox noninnocence has been established. Both EPR and UV−vis spectra exhibit all of the characteristic traits of a coordinated phenoxyl radical when **2** is oxidized. The Mulliken spin population analysis deposits spin density almost exclusively on the phenolate arms of $(L^{\bullet})^{1-}$ in $[\mathbf{2}]^+$ and $[\mathbf{2}]^{2+}$, with little change in the geometry optimized intraligand bond distances. This is the first time that two radical ligands have been observed coordinated in a dimeric species to afford a singlet diradical.

Acknowledgment. N.R. and S.S. are grateful to the Max Planck Society for a doctoral stipend and postdoctoral fellowship, respectively. We thank the Fonds der Chemischen Industrie for financial support.

Supporting Information Available: X-ray crystallographic files in CIF format for $H_2(L-L)$, **1**, and **2**. Cyclic voltammogram, electronic absorption, and zero-field Mössbauer spectrum of **1**. Tables of geometrical and electronic structural details of DFT calculations for **1** and **2**, including Mulliken spin density plots of **1** and $[\mathbf{1}]^+$, and MO manifold diagrams for **1** and $[\mathbf{2}]^+$. This material is available free of charge via the Internet at http://pubs.acs.org.

IC8023716